Computational Materials Science 210 (2022) 111434

Contents lists available at ScienceDirect

Computational Materials Science

journal homepage: www.elsevier.com/locate/commatsci

Full length article

DefAP: A Python code for the analysis of point defects in crystalline solids

William D. Neilson, Samuel T. Murphy *

Engineering Department, Lancaster University, Bailrigg, Lancaster, LA1 4YW, UK

ARTICLE INFO

Keywords:
Defect chemistry
Thermodynamics
Brouwer diagrams

ABSTRACT

Inevitably, all crystalline materials will contain imperfections that have the ability to modify the properties of the host material. Key to the development of advanced materials is the ability to predict the concentrations of different defects in any given environmental conditions and how the change in the defect population alters the material's properties. Modern first principles atomistic simulation techniques, such as density functional theory (DFT), are now widely employed for the simulation of point defects, however, to develop true insight into a material's defect chemistry, it is essential to link the energies calculated to thermodynamic variables that fully describe its operating conditions. The Defect Analysis Package (DefAP), an open-source Python code, has been designed to fulfil this role. The primary function of the package is to predict the concentrations of defects in materials as a function of key thermodynamic variables, such as temperature and availability of different species, expressed through chemical potentials. Through simple thermodynamic equations, DefAP allows the rapid exploration of a material's defect chemistry allowing direct comparison with experimental observations. Rapid exploration is supported through the use of autoplotting with carefully considered automatic data labelling and simplification options enabling production of publication quality plots. DefAP offers a wide range of options for the calculation of defect and carrier concentrations that can be customised by the user to suit the material studied and an extensive suite of options have been designed for the study of extrinsic defects (e.g. dopants or impurities). The capabilities of DefAP are demonstrated in this paper by studying intrinsic defects in $YBa_2Cu_3O_7$, P doping in Si, Am accumulation in PuO_2, and simultaneous build-up of T and He in Li_2TiO_3.

1. Introduction

An understanding of the underlying point defect processes responsible for the macroscopic properties of materials is fundamental to the development of higher performance materials [1]. A "defect" can be considered to be any localised disruption to the perfect crystal lattice and are typically categorised according to their dimensionality, i.e. point defects (0D), dislocations (1D), surfaces/grain boundaries (2D) and bubbles/voids (3D). Despite their small size, point defects play a crucial role in the conductivity of semiconductors, the efficiency of solar cells and related optoelectronic devices, and the degradation of properties of metal oxide nuclear fuels during operation. As illustrated in these examples, the presence of defects is deleterious when a pure material is desired, but through careful manipulation they can be used to enhance specific properties [2]. In addition to intrinsic defect species, point defects play a crucial role in the incorporation of dopant species. The incorporation of foreign atoms into a material, whether intentionally doped or naturally occurring (e.g. radiogenic species), can produce dramatic changes to a material's characteristics.

The fundamental requirement is to be able to determine a material's defect concentrations and how the presence of these defects may modify the properties of the material. While there are a wide array of experimental techniques that are able to infer the presence of different types of defects in a material, an estimation of their concentration is still challenging. In recent years, the dramatic increase in computational power has enabled the study of point defects in materials using *ab initio* techniques such as Density Functional Theory (DFT) [3]. Such simulations are now routine and an excellent guide is given by Kim et al. [4], however, potential users should be aware of the complexities surrounding the use of DFT for the simulations of defects [5]. Within a DFT simulation the defect is introduced into a relatively small supercell, typically in the region of 100s of atoms, which is then relaxed allowing the calculation of an energy. In order to gain useful physical insight this energy must be combined with thermodynamics to adequately describe the material's environment. This is crucial as the concentration of a defect in a material will depend on factors including the availability of atoms/ions, temperature, pressure etc. Given the defect concentrations are not constant this further implies that there is no single value for the

* Corresponding author.
E-mail address: samuel.murphy@lancaster.ac.uk (S.T. Murphy).

https://doi.org/10.1016/j.commatsci.2022.111434
Received 19 January 2022; Received in revised form 4 April 2022; Accepted 5 April 2022
Available online 5 May 2022

defect formation energy — they too depend on these factors. Therefore, what is required is a convenient method for linking the results of DFT simulations with appropriate thermodynamics.

The Defect Analysis Package (DefAP), an open-source Python code, has been developed to facilitate the exploration of a material's defect chemistry, connecting the results of DFT calculations with bespoke, user-customised thermodynamics and processing operations that can be tailored to any defect-containing system of interest. At its core, DefAP is designed to calculate defect formation energies and concentrations under a range of different experimental conditions, with finite-size effects (due to small simulation cells) mitigated with the optional use of a point charge correction that is applicable to both isotropic and anisotropic systems.

Alternative codes are available that offer post-treatment of defect-DFT calculations. Some focus on the evaluation of a defect's formation energy [6,7], whilst the codes Spinney [8], PyDEF-2.0 [9] and SC-FERMI [10] also offer the capability to calculate carrier and defect concentrations. In this paper we outline the enhanced capabilities that makes DefAP an attractive alternative to these codes. DefAP is designed to be user friendly; uniquely, it can perform the calculation of the formation energy of multiple defects and their corresponding equilibrium concentrations as a function of a chosen environmental variable in one single operation, with automatic production of attractive, publication quality plots, using gnuplot.

Examples of the user-customisable methodology include the choice of method to calculate carrier concentrations (to suit the system being studied), the modelling of chemical potential temperature dependence using a real gas model, and the option to consider the change in vibrational entropy due to the defect when calculating the defect's formation energy. The ability to study controlled quantities of multiple dopant species is available, where DefAP determines the chemical potential of each dopant element that delivers the user-defined concentration of each dopant species. This is possible for multiple dopant elements for the first time, due to the nonlinear optimiser designed in the code.

In Section 2 we outline the methodology and formalism of the DefAP code, before demonstrating the capabilities and usage of the code in Section 3, with use of example systems.

2. Methodology

In this section, we detail the scientific principles that DefAP uses throughout its calculations. We use the superscript 'DFT' to denote terms that would be obtained by the user using a DFT code; DefAP is not tied to one specific code (VASP, CASTEP, etc.) but one code must of course be used consistently. For a comprehensive description of how a user would operate DefAP, we refer the reader to the manual.

Point defects, e.g. vacancies, interstitials, and substitutionals, are crystallographic defects that occur at or around a single lattice point. Assuming that the number of point defects is small compared to the number of lattice sites in the crystal, the equilibrium concentration, c_i, of defect i can be related to the change in the Gibbs free energy, $\Delta G_\mathrm{f}^\mathrm{i}$, to form the defect, i. Using simple Boltzmann statistics this relationship can be represented as [11]:

$$c_i = m_i \exp\left(\frac{-\Delta G_\mathrm{f}^i}{k_\mathrm{B}T}\right) \tag{1}$$

where, m_i is the multiplicity of equivalent sites, k_B is the Boltzmann constant and T is the temperature. Eq. (1) is derived assuming that defect concentrations are small, where interactions between defects are negligible. The energies of the perfect and defective cells are used to define $\Delta G_\mathrm{f}^\mathrm{i}$ as:

$$\Delta G_\mathrm{f}^i = E_\mathrm{defect}^\mathrm{DFT} - E_\mathrm{perfect}^\mathrm{DFT} - T\Delta S_\mathrm{vib} \pm \sum_\alpha n_\alpha \mu_\alpha + q_\mathrm{i}\mu_\mathrm{e} + E_\mathrm{corr} \tag{2}$$

$E_\mathrm{defect}^\mathrm{DFT}$ and $E_\mathrm{perfect}^\mathrm{DFT}$ are the DFT total energies of the system with and without the defect, i. ΔS_vib is the difference in vibrational entropy between defective and perfect supercells and is discussed in Section 2.3. The contribution of vibrational entropy to the defect formation energy is significant and should not be neglected, especially at high temperatures. The contribution can however be neglected if desired, and it is widely considered safe to do so at relatively low temperatures. If neglected, the term $\Delta G_\mathrm{f}^\mathrm{i}$ is replaced with $\Delta E_\mathrm{f}^\mathrm{i}$. n_α is the number of atoms of species, α, added to or removed from the system to make defect i, μ_α is the chemical potential of species α and $\mu_\mathrm{e} = E_\mathrm{VBM} + \varepsilon_\mathrm{F}$. E_VBM is the energy of the valence band maximum (VBM) and ε_F is the electron chemical potential above the VBM. E_corr is an optional correction used to mitigate charge interactions of the defect charges with their periodic images. There have been a large number of charge corrections developed [12–18], however, many of these require the further examination of the output from DFT calculation of each defect. The resulting corrections can be input manually or DefAP offers the ability to automatically include a point charge correction, as discussed in Section 2.4.

More recently Kasamatsu et al. [19] have derived a more complex expression for the concentration of a given defect, which includes the interactions of defects competing for the same lattice sites, that is:

$$c_i = m_i \frac{\exp\left(\frac{-\Delta E_\mathrm{f}^i}{k_\mathrm{B}T}\right)}{1 + \sum_j \exp\left(\frac{-\Delta E_\mathrm{f}^j}{k_\mathrm{B}T}\right)} \tag{3}$$

where, the sum in the denominator is performed over all defects that occupy the same lattice site as defect i. DefAP allows choice of the expression used to calculate defect concentrations, at low defect concentrations (i.e. when $\Delta E_\mathrm{f} \ll k_\mathrm{B}T$) the two expressions converge as there is little competition for lattice sites.

A key design principle of the code is the ability to, in a single operation, evaluate a material's defect chemistry over a range of conditions. DefAP evaluates Eqs. (1) or (3), & (2) at *iterations* taken between a *minimum* and *maximum* value of a *property* (where italicised values are user-defined). The properties that can be selected are either (1) the partial pressure of a volatile species, (2) temperature, (3) the concentration of a dopant, or (4) the concentration of an artificial dopant. Dopants are discussed in Section 2.5.

2.1. Chemical potentials

DefAP contains several mechanisms to either input or calculate the chemical potentials of the elements in the system under study. The user must select one of the four mechanisms implemented in DefAP, based upon the nature of the system studied. The first of these four mechanisms is appropriate for the study of simple systems such as semiconductors (e.g. Si) where the chemical potentials are calculated using DFT or other external means, and supplied in the input file. The only requirement to using this mechanism is that the defined chemical potentials for the constituent elements, as entered, add up to that for the host system, a check that is performed by DefAP. Using $\mathrm{M}_\alpha\mathrm{N}_\beta$ as an example, the following criteria must be met:

$$\alpha\mu_{\mathrm{M_{(s)}}} + \beta\mu_{\mathrm{N_{(s)}}} = \mu^\mathrm{DFT}_{\mathrm{M}_\alpha\mathrm{N}_{\beta\,\mathrm{(s)}}} \tag{4}$$

The second mechanism, used for systems that contain multiple metal species, enables the exploration of the defect chemistry under conditions that contain either an excess or deficit of each of the species (referred to here as rich and poor conditions, respectively). Again, using the example system $\mathrm{M}_\alpha\mathrm{N}_\beta$, the rich condition for each specie is determined using DFT, i.e.:

$$\mu_\mathrm{M}^\mathrm{M-rich} = \mu^\mathrm{DFT}_{\mathrm{M_{(s)}}} \tag{5}$$

To calculate the chemical potential of each element under poor conditions, we assume all other elements are defined to be in their rich condition, for example:

$$\mu_\mathrm{M}^\mathrm{M-poor} = \frac{\mu^\mathrm{DFT}_{\mathrm{M}_\alpha\mathrm{N}_{\beta\,\mathrm{(s)}}} - \beta\mu^\mathrm{DFT}_{\mathrm{N_{(s)}}}}{\alpha} \tag{6}$$

We therefore now have a range in the chemical potential for each element, from poor to rich conditions. To access intermediate compositions we define a fraction, f, for each metal in the system which is used to calculate the chemical potential of each element, e.g.:

$$\mu_{\mathrm{M}}^{f} = f\,\mu_{\mathrm{M}}^{\mathrm{M-rich}} + (1-f)\mu_{\mathrm{M}}^{\mathrm{M-poor}} \tag{7}$$

A limitation is placed on the possible fractions, f, assigned to each element:

$$\sum_{j} f^{j} = n - 1 \tag{8}$$

where n is the number of metal elements in the system. For the example system discussed here, $\mathrm{M}_{\alpha}\mathrm{N}_{\beta}$, n equals 2, necessitating that $f^{M} + f^{N} = 1$. If f^{M} is set to equal 1, the system would be M-rich meaning that $f^{N} = 0$ and so the system would be at the N-poor limit.

Compounds containing an element that is in the gas phase in its standard state are systems routinely subject to defect chemistry studies. For such compounds that are binary, the third mechanism is designed to calculate the chemical potential of both constituent elements. We express these generally as $\mathrm{M}_{\alpha}\mathrm{V}_{\beta}$, where V is a volatile element that exists naturally as a binary gas molecule (O, N, H, Cl and F are common examples that could be V). The chemical potential of V is dependent on the partial pressure of V and on temperature, which results in the chemical potential of M depending on these variables too. To calculate the chemical potentials of the elements in this type of system, DefAP begins by decomposing the binary compounds into their constituents, for example, for $\mathrm{M}_{\alpha}\mathrm{V}_{\beta}$:

$$\alpha\mu_{\mathrm{M_{(s)}}} + \beta\mu_{\mathrm{V}}(P_{\mathrm{V_2}}, T) = \mu^{\mathrm{DFT}}_{\mathrm{M}_{\alpha}\mathrm{V}_{\beta(\mathrm{s})}} \tag{9}$$

To determine the chemical potential of V the approach of Finnis et al. [20] is adopted. This method uses the known formation energy of the binary compound under standard conditions, $\Delta G_{\mathrm{f}}^{\mathrm{M}_{\alpha}\mathrm{V}_{\beta}}(P^{\circ}_{\mathrm{V_2}}, T^{\circ})$, to obtain the chemical potential of V at standard temperature and pressure:

$$\Delta G_{\mathrm{f}}^{\mathrm{M}_{\alpha}\mathrm{V}_{\beta}}(P^{\circ}_{\mathrm{V_2}}, T^{\circ}) = \mu^{\mathrm{DFT}}_{\mathrm{M}_{\alpha}\mathrm{V}_{\beta(\mathrm{s})}} - \alpha\mu^{\mathrm{DFT}}_{\mathrm{M_{(s)}}} - \beta\mu_{\mathrm{V}}(P^{\circ}_{\mathrm{V_2}}, T^{\circ}) \tag{10}$$

The chemical potential of V at the desired conditions, $\mu_{\mathrm{V}}(P_{\mathrm{V_2}}, T)$, is extrapolated from $\mu_{\mathrm{V}}(P^{\circ}_{\mathrm{V_2}}, T^{\circ})$ using Eq. (11):

$$\mu_{\mathrm{V}}(P_{\mathrm{V_2}}, T) = \mu_{\mathrm{V}}(P^{\circ}_{\mathrm{V_2}}, T^{\circ}) + \Delta\mu(T) + \frac{1}{2}k_{\mathrm{B}}T\left(\frac{P_{\mathrm{V_2}}}{P^{\circ}_{\mathrm{V_2}}}\right) \tag{11}$$

$\Delta\mu(T)$ represents the temperature contribution to the chemical potential. DefAP contains two different approaches for the user to choose when calculating this contribution; the first option is to treat $\mathrm{V_2}$ as a rigid-dumbbell ideal gas and use the following equation:

$$\Delta\mu(T) = -\frac{1}{2}(S^{\circ}_{\mathrm{V_2}} - C^{\circ}_{P}) + C^{\circ}_{P}T\log\left(\frac{T}{T^{\circ}}\right) \tag{12}$$

where $S^{\circ}_{\mathrm{V_2}}$ is the molecular entropy at standard temperature and pressure and C°_{P} is the constant pressure heat capacity of $\mathrm{V_2}$. The values DefAP uses for these two properties are taken from the National Institute of Standards and Technology (NIST) Chemistry WebBook [21]; $\mathrm{O_2}$, $\mathrm{N_2}$, $\mathrm{H_2}$, $\mathrm{Cl_2}$ and $\mathrm{F_2}$ are the implemented options. The alternative option is to calculate $\Delta\mu(T)$ using the real heat capacities of the $\mathrm{V_2}$ molecule and employ the Shomate equations:

$$\Delta\mu(T) = \frac{1}{2}(G(P^{\circ}, T) - G(P^{\circ}, T^{\circ})) \tag{13}$$

where,

$$G(P^{\circ}, T) = H(P^{\circ}, T) - TS(P^{\circ}, T) \tag{14}$$

$$H(P^{\circ}, T) = 1000(At + \frac{1}{2}Bt^2 + \frac{1}{3}Ct^3 - \frac{1}{4}Dt^4 - \frac{E}{t} + F - H) \tag{15}$$

$$S(P^{\circ}, T) = A\ln(t) + Bt + \frac{1}{2}Ct^2 + \frac{1}{3}Dt^3 - \frac{E}{2t^2} + G \tag{16}$$

$$t = \frac{T(K)}{1000} \tag{17}$$

Eqs. (15)–(17) and the temperature-dependent parameters $A - G$ are taken from the NIST Chemistry WebBook [21]. Again, $\mathrm{O_2}$, $\mathrm{N_2}$, $\mathrm{H_2}$, $\mathrm{Cl_2}$ and $\mathrm{F_2}$ are the implemented options.

The final mechanism implemented in DefAP is designed to calculate the chemical potential of constituent elements in systems containing a volatile element and multiple metal species, i.e. a non-binary volatile compound. To do this, we deconstruct the compound into binary volatile compounds that could be assumed to thermodynamically construct the original compound. Using the compound $\mathrm{M}_{\alpha}\mathrm{N}_{\beta}\mathrm{V}_{\gamma}$ as an example, where V is the volatile element, we can say:

$$\mathrm{AM}_{\delta}\mathrm{V}_{\epsilon(\mathrm{s})} + \mathrm{BN}_{\zeta}\mathrm{V}_{\eta(\mathrm{s})} + \frac{1}{2}\mathrm{CV}_{2(\mathrm{g})} \rightarrow \mathrm{M}_{\alpha}\mathrm{N}_{\beta}\mathrm{V}_{\gamma(\mathrm{s})} \tag{18}$$

where,

$$\delta\mathrm{A} = \alpha \tag{19}$$

$$\zeta\mathrm{B} = \beta \tag{20}$$

$$\epsilon\mathrm{A} + \eta\mathrm{B} + \mathrm{C} = \gamma \tag{21}$$

Under any given conditions, the sum of the chemical potentials per formula unit of the constituent species must be equal to the total Gibbs free energy of the host compound, i.e. in our example:

$$\mathrm{A}\mu_{\mathrm{M}_{\delta}\mathrm{V}_{\epsilon}}(P_{\mathrm{V_2}}, T) + \mathrm{B}\mu_{\mathrm{N}_{\zeta}\mathrm{V}_{\eta}}(P_{\mathrm{V_2}}, T) + \mathrm{C}\mu_{\mathrm{V}}(P_{\mathrm{V_2}}, T) = \mu_{\mathrm{M}_{\alpha}\mathrm{N}_{\beta}\mathrm{V}_{\gamma(\mathrm{s})}} \tag{22}$$

Under standard conditions it is assumed that $\mu_{\mathrm{M}_{\alpha}\mathrm{N}_{\beta}\mathrm{V}_{\gamma}}(P_{\mathrm{V_2}}, T) = \mu_{\mathrm{M}_{\alpha}\mathrm{N}_{\beta}\mathrm{V}_{\gamma(\mathrm{s})}}$, where the chemical potential of $\mathrm{M}_{\alpha}\mathrm{N}_{\beta}\mathrm{V}_{\gamma}$ is calculated using DFT. Under equilibrium conditions, the chemical potentials of the constituents of a crystal cannot exceed the Gibbs free energy of any phase made of the constituent elements. For example, the chemical potential of $\mathrm{M}_{\delta}\mathrm{V}_{\epsilon}$ in $\mathrm{M}_{\alpha}\mathrm{N}_{\beta}\mathrm{V}_{\gamma}$ cannot exceed that of solid $\mathrm{M}_{\delta}\mathrm{V}_{\epsilon}$, otherwise a $\mathrm{M}_{\delta}\mathrm{V}_{\epsilon}$ precipitate would form. The approach DefAP adopts to find the chemical potentials is to set upper and lower bounds for each binary compound that is selected in Eq. (18). However there may be many other possible phases that the host compound could decompose into, in addition to the binary compounds in Eq. (18). Functionality exists in DefAP to examine the stability of these competing phases and is discussed in Section 2.1.1. Returning to the determination of chemical potentials, we set the upper bound for the chemical potential of each binary compound using DFT, using $\mathrm{M}_{\delta}\mathrm{V}_{\epsilon}$ as an example:

$$\mu^{\mathrm{M}_{\delta}\mathrm{V}_{\epsilon}-\mathrm{rich}}_{\mathrm{M}_{\delta}\mathrm{V}_{\epsilon}} = \mu^{\mathrm{DFT}}_{\mathrm{M}_{\delta}\mathrm{V}_{\epsilon(\mathrm{s})}} \tag{23}$$

To calculate the lower bound for the chemical potential each binary compound, we assume all other binary compounds must be at their upper bound and thus:

$$\mu^{\mathrm{M}_{\delta}\mathrm{V}_{\epsilon}-\mathrm{poor}}_{\mathrm{M}_{\delta}\mathrm{V}_{\epsilon}} = \frac{\mu^{\mathrm{DFT}}_{\mathrm{M}_{\alpha}\mathrm{N}_{\beta}\mathrm{V}_{\gamma(\mathrm{s})}} - \mathrm{B}\mu^{\mathrm{DFT}}_{\mathrm{N}_{\zeta}\mathrm{V}_{\eta(\mathrm{s})}} - \mathrm{C}\mu_{\mathrm{V}}(P_{\mathrm{V_2}}, T)}{\mathrm{A}} \tag{24}$$

The values for the chemical potentials can fall anywhere in this rich/poor range, therefore we define a fraction, f, for each binary compound which controls where in this range the chemical potential falls:

$$\mu^{f}_{\mathrm{M}_{\delta}\mathrm{V}_{\epsilon}} = f\,\mu^{\mathrm{M}_{\delta}\mathrm{V}_{\epsilon}-\mathrm{rich}}_{\mathrm{M}_{\delta}\mathrm{V}_{\epsilon}} + (1-f)\mu^{\mathrm{M}_{\delta}\mathrm{V}_{\epsilon}-\mathrm{poor}}_{\mathrm{M}_{\delta}\mathrm{V}_{\epsilon}} \tag{25}$$

The fractions, f, assigned to each binary compound must be such that Eq. (8) is obeyed. The calculated chemical potentials of the binary oxides are further decomposed into the constituent elements according to the method outlined previously using Eqs. (9)–(17). This method calculates a chemical potential of V at standard temperature and pressure ($\mu_{\mathrm{V}}(P^{\circ}_{\mathrm{V_2}}, T^{\circ})$) for each binary compound selected in Eq. (18). A final value of $\mu_{\mathrm{V}}(P^{\circ}_{\mathrm{V_2}}, T^{\circ})$ is calculated by DefAP as a weighted average of the contributions by the fractions of binary compounds present:

$$\mu_{\mathrm{V}}(P^{\circ}_{\mathrm{V_2}}, T^{\circ}) = \frac{1}{n-1}\sum_{j} f^{j}\mu^{j}_{\mathrm{V}}(P^{\circ}_{\mathrm{V_2}}, T^{\circ}) \tag{26}$$

2.1.1. Thermodynamic stability

As discussed throughout this section, DefAP relies on the DFT energies of reference compounds to calculate the chemical potentials of each compounds constituent elements. This approach ensures that each of the selected reference compounds are thermodynamically stable with respect to the host system; using $M_\alpha V_\gamma$ as an example of a reference compound in the host system, $M_\alpha N_\beta V_\gamma$, Eq. (28) is satisfied:

$$\alpha\mu_{M_{(s)}} + \gamma\mu_V(P_{V_2}, T) \leq \mu^{DFT}_{M_\alpha V_{\gamma(s)}} \tag{27}$$

However, many systems will posses a multitude of possible compounds, not used as a reference compound, that the host system could potentially decompose to under specific conditions. DefAP offers the capability to predict the stability of the system with respect to any number of compounds under the range of conditions investigated. For example, the criteria for the stability of $M_\alpha N_\beta V_\gamma$ with respect to M_2V_3 would be that:

$$2\mu_{M_{(s)}} + 3\mu_V(P_{V_2}, T) \leq \mu^{DFT}_{M_2V_{3(s)}} \tag{28}$$

In this example, the user would supply the DFT energy of M_2V_3. If, after DefAP calculates $\mu_{M_{(s)}}$ and $\mu_V(P_{V_2}, T)$ at a given condition, Eq. (28) is not satisfied, a warning will be given. The user may then choose to appropriately adjust their defined position in chemical potential space or the requested environmental conditions. It must be noted that DefAP can only provide an indicator of the thermodynamic stability of a phase; a phase predicted to be unstable would not necessarily be able to overcome the kinetic barriers needed to form a secondary phase. It is for this reason a warning is given instead of terminating the program.

2.2. Electron and hole concentrations

In charged systems, the sum of the concentrations of ionic and electronic defects, each multiplied by their charges, must balance to provide overall charge neutrality. This can be expressed as:

$$\sum_i q_i c_i - c_{e^-} + c_{p^+} = 0 \tag{29}$$

The first term is the sum of the charges of the point defects. The second and third terms correspond to the concentrations of electrons (e^-) and holes (p^+) respectively. DefAP offers the user several options to calculate the concentration of the electronic defects. The first of these options is to simply fix the concentrations at a desired value. The second option is to employ Boltzmann statistics, with use of Eqs. (30) and (31).

$$c_{e^-} = N_c \exp\left(-\frac{E_g - \varepsilon_F}{k_B T}\right) \tag{30}$$

$$c_{p^+} = N_v \exp\left(-\frac{\varepsilon_F}{k_B T}\right) \tag{31}$$

N_c and N_v are the effective conduction band and valence band density of states (DOS) and E_g is the bandgap. The third option to calculate electronic defect concentrations is to apply Fermi–Dirac statistics to the electronic DOS to obtain the concentrations of e^- in the conduction band and concentration of holes p^+ in the valance band, respectively:

$$c_{e^-} = \int_{E_{CBM}}^{\infty} g_c(E) \frac{dE}{1 + \exp(\frac{E - \varepsilon_F}{k_B T})} \tag{32}$$

$$c_{p^+} = \int_{-\infty}^{E_{VBM}} g_v(E) \frac{dE}{1 + \exp(\frac{\varepsilon_F - E}{k_B T})} \tag{33}$$

$g_c(E)$ and $g_v(E)$ are the density of electronic states in the conduction band and valence band, respectively. E_{CBM} is the energy of the conduction band minimum. We advocate the use of Fermi–Dirac statistics over Boltzmann statistics owing to the direct utilisation of the systems' DOS. A final option which is particularly useful for the study of semiconductors is to return to Eqs. (30) and (31) but to transform N_c and N_v to the DOS effective mass of electrons and holes, respectively. N_c and N_v are now calculated using the following equations:

$$N_c = 2\left(\frac{2\pi m_e^* k_B T}{h^2}\right)^{\frac{3}{2}} \tag{34}$$

$$N_v = 2\left(\frac{2\pi m_p^* k_B T}{h^2}\right)^{\frac{3}{2}} \tag{35}$$

m_e^* and m_p^* are the electron and hole effective mass in the chosen semiconductor, respectively. h is Planck's constant. Altogether, in charged systems, there remains one variable in Eq. (29) that DefAP is designed to compute: the Fermi level that achieves charge neutrality. The convergence criteria for charge neutrality is set by default to be very low ($< 10^{-10}u$), but can be adjusted by the user to further increase accuracy as detailed in the manual. DefAP also checks that the Fermi level computed falls within the bandgap.

2.3. Vibrational entropy

DefAP enables the consideration of the difference in vibrational entropy between defective and perfect supercells when evaluating the formation energy of each defect. The vibrational entropy of a system is temperature dependent, therefore DefAP uses interpolation to calculate the vibrational entropy of the system at the desired temperature. This requires the user to gather the vibrational entropy of defective and perfect systems at several temperature values. At the time of writing, phonon calculations of defect-containing supercells are very expensive in DFT. A successful strategy adopted in past studies has seen empirical potentials used to calculate vibrational entropies [22–25]. In addition to the inclusion of the vibrational entropy term in Eq. (2), if the chemical potentials have dependence on temperature (i.e. a volatile element is in the system), modifications are made to the method that chemical potentials are calculated. Using $S_x(T)$, the vibrational entropy of compound x at temperature T, Eq. (9) is modified to:

$$\alpha\mu_{M_{(s)}} + \beta\mu_V(P_{V_2}, T) = \mu^{DFT}_{M_\alpha V_{\beta(s)}} - TS_{M_\alpha V_{\beta(s)}}(T) \tag{36}$$

Eqs. (23) and (24), employed when studying non-binary volatile compounds, are modified to Eqs. (37) and (38), respectively.

$$\mu^{M_\delta V_\epsilon\text{-rich}}_{M_\delta V_\epsilon} = \mu^{DFT}_{M_\delta V_{\epsilon(s)}} - TS_{M_\delta V_{\epsilon(s)}}(T) \tag{37}$$

$$\mu^{M_\delta V_\epsilon\text{-poor}}_{M_\delta V_\epsilon} = \frac{\mu^{DFT}_{M_\alpha N_\beta V_{\gamma(s)}} - TS_{M_\alpha N_\beta V_{\gamma(s)}}(T) - B\left(\mu^{DFT}_{N_\zeta V_{\eta(s)}} - TS_{N_\zeta V_{\eta(s)}}(T)\right) - C\mu_V(P_{V_2}, T)}{A} \tag{38}$$

2.4. Finite size error corrections

The introduction of charged defects into the small simulation supercells accessible using DFT introduces a number of finite size effects as discussed extensively in Ref. [26]. These include Coulombic interactions between the defect and its periodic image as well as with the background charge. The result is that defect formation energies exhibit a strong dependence on the size of the supercell used and this must be corrected for. DefAP offers the option for externally calculated corrections for each defect to be supplied and used, or, alternatively the direct calculation and implementation of the correction for each defect. The charge correction that DefAP can calculate for a simple point charge is given as:

$$E_{corr} = \frac{q^2 v_M^{scr}}{2} = \frac{q^2 \alpha}{2\epsilon L} \tag{39}$$

where, v_M^{scr} is the Madelung potential for a point charge in a general 3-dimensional box screened by a general dielectric. If the system is

cubic, $v_M^{scr} = \frac{\alpha}{\epsilon L}$, where $\alpha = 2.837$, L is the length of the simulation supercell and ϵ is the material's dielectric constant. If studying a non-cubic system with anisotropic dielectric properties, DefAP can be used to calculate an appropriate value of v_M^{scr} for the system, using the systems dielectric tensor, $\bar{\epsilon}$, and the method described by Murphy and Hine [17]:

$$v_M^{scr} = \sum_{\mathbf{R}_i}^{i\neq 0} \frac{1}{\sqrt{\det \bar{\epsilon}}} \frac{\mathrm{erfc}(\gamma\sqrt{\mathbf{R}_i \cdot \bar{\epsilon}^{-1} \cdot \mathbf{R}_i})}{\sqrt{\mathbf{R}_i \cdot \bar{\epsilon}^{-1} \cdot \mathbf{R}_i}} + \sum_{\mathbf{G}_i}^{i\neq 0} \frac{4\pi}{V_c} \times \frac{\exp(-\mathbf{G}_i \cdot \bar{\epsilon} \cdot \mathbf{G}_i / 4\gamma^2)}{\mathbf{G}_i \cdot \bar{\epsilon} \cdot \mathbf{G}_i} - \frac{2\gamma}{\sqrt{\pi \det \bar{\epsilon}}} - \frac{\pi}{V_c \gamma^2} \tag{40}$$

where the sum extends over all vectors of the direct ($\mathbf{R}_i$) and reciprocal ($\mathbf{G}_i$) lattices, γ is a suitably chosen convergence parameter, and V_c is the volume of the supercell.

2.5. Dopants and impurities

Many of the most interesting properties of materials arise due to the presence of foreign atoms in the host matrix, whether this is due to intentional doping or unintentionally such as accommodation of fission products in a nuclear fuel. When considering dopants there are two major factors to consider, the first is how the foreign atoms are incorporated into the lattice and second how does the presence of the foreign atom influence the intrinsic defect chemistry. There are two different methods for studying dopants in DefAP. The first and most simple is to introduce a concentration of defects with a given charge. In this case the type of defect that is incorporated is not important, however this allows the user to see how the introduction of say 1 ppm of a defect with a 1+ charge alters the concentrations of the intrinsic defects. The charge neutrality condition, Eq. (29), is modified to accommodate the artificial presence of a dopant with concentration, c_D, and charge, q_D:

$$\sum_i q_i c_i - c_{e^-} + c_{p^+} + c_D q_D = 0 \tag{41}$$

The advantage of this approach is that it does not require any further DFT data, however, there is no insight about how the foreign atoms are accommodated in the lattice. In the second approach, the dopant is included by considering its incorporation as a defect at different lattice sites using DFT, then calculating the formation energy of each considered defect with Eq. (2). This approach requires the calculation of the chemical potential for the dopant. There are two possibilities for defining the chemical potential of the dopant, dependent on the source of the dopant. The first option considers a constant, unlimited source/reservoir, with the result being a description of how the host lattice incorporates the dopant from this reservoir. The dopant chemical potential, $\mu_{\mathrm{D_{(s)}}}$, is calculated from a supplied reference state compound; for example, $\mathrm{D}_\alpha\mathrm{V}_\beta$, containing the dopant element, D, and a volatile element present in the host system, V:

$$\mu_{\mathrm{D_{(s)}}} = \frac{\mu^{\mathrm{DFT}}_{\mathrm{D}_\alpha\mathrm{V}_{\beta(\mathrm{s})}} - \beta\mu_{\mathrm{V}}(P_{\mathrm{V}_2}, T)}{\alpha} \tag{42}$$

The reference state compound can be replaced with a reference dopant atom as appropriate for gasses, such as Xe. The second option for determining the dopant chemical potential is to define the total concentration of the dopant as a specified, restricted quantity that exists in the material. DefAP determines the dopant chemical potential and blend of dopant defects that delivers the desired concentration. This is a very useful method as often the concentration of a dopant under experimental conditions is known/desired and an inquiry exists regarding the accommodation of this concentration. Examples include semiconductors doped with specific concentrations of dopant elements or nuclear fuels containing known quantities of radiogenic impurities.

If one dopant element is studied, DefAP uses linear bisection to find the chemical potential of the dopant that achieves the desired concentration, subject to the constraint that, if a charged system is being studied, the Fermi level is in the bandgap. DefAP can also study systems with multiple dopant elements, each with a specified concentration target. This becomes a nonlinear optimisation, therefore, sequential least squares programming (SLSQP) is deployed to find a solution, subject to the Fermi level constraint, described above. The thermodynamic stability of secondary phases that include elements of the dopant(s) can be investigated using the same methodology described in Section 2.1.1.

2.6. Stoichiometry deviation

When studying compounds that contain an element that is in the gas phase in its standard state, the ratio of this volatile element to the metal element(s) (or the stoichiometry) is of particular interest. Deviations in stoichiometry may a have significant impact upon the material properties, for example, the oxygen-to-metal ratios in metal oxide nuclear fuels are a critical parameter of performance. Small deviations in perfect stoichiometry can result from the formation of point defects; DefAP calculates the concentration of these defects, enabling a measurement and prediction of both the magnitude and cause of any deviation. No additional information is needed from the user, and the program is able to calculate the stoichiometry for both binary and non-binary compounds. Here, to aid description of the method DefAP uses to calculate any deviation, a binary compound, $\mathrm{M}_\alpha\mathrm{V}_{\beta\pm x}$, can be considered where M is a metal element, V is the volatile element and x is the deviation from stoichiometry. Again, this represents a binary compound, but there may be multiple metal species if a non-binary compound is studied. To calculate the value of x, the compound of interest is rewritten in the form, $\mathrm{M}_{\alpha+y}\mathrm{V}_{\beta+z}$, where y and z represent the surplus of M and V, as a result of the formation of defects, respectively. To calculate x, we use Eq. (43), where α and y are computed for each metal species, m.

$$\beta + x = \frac{\beta + z}{\sum_m (\alpha + y)} \tag{43}$$

z and y are calculated using the predicted defect concentrations; the concentration of defects that involve the addition of the volatile element to the host contribute positively to z, conversely the concentration of defects that involve the removal of the volatile element are subtracted from z. y is the metal equivalent of z, but if the number of metal species in the host exceeds one, y is calculated for each species individually.

The addition of dopant/impurity element(s), D, to the host invokes reconsideration of the method used to calculate x in the compound $\mathrm{M}_\alpha\mathrm{D}_w\mathrm{V}_{\beta\pm x}$. If dopant defects are studied, two options are available to calculate the deviation in stoichiometry. The first is to retain use of Eq. (43) which considers the cation/volatile species leaving the system as a consequence of the dopant addition when calculating z and y in $\mathrm{M}_{\alpha+y}\mathrm{D}_w\mathrm{V}_{\beta+z}$, but does not treat the dopant as a cation species, (i.e. the value of w is insignificant). Alternatively, the second option treats the dopant species as metal species, with x in $\mathrm{M}_\alpha\mathrm{D}_w\mathrm{V}_{\beta\pm x}$ calculated using Eq. (44) which includes the term w. w is calculated separately for each dopant species, d, and is the sum of the concentration of defects that include the dopant species.

$$\beta + x = \frac{\beta + z}{\sum_m (\alpha + y) + \sum_d w} \tag{44}$$

3. Example usage

In this section we highlight the capabilities of DefAP by studying the defect chemistry of four systems: Si, PuO_2, $YBa_2Cu_3O_7$, and Li_2TiO_3. The effect of P incorporation into Si, Am in PuO_2, and both T and He in Li_2TiO_3 is investigated to showcase the study of dopant defects. These systems help demonstrate the output of DefAP, however, a detailed

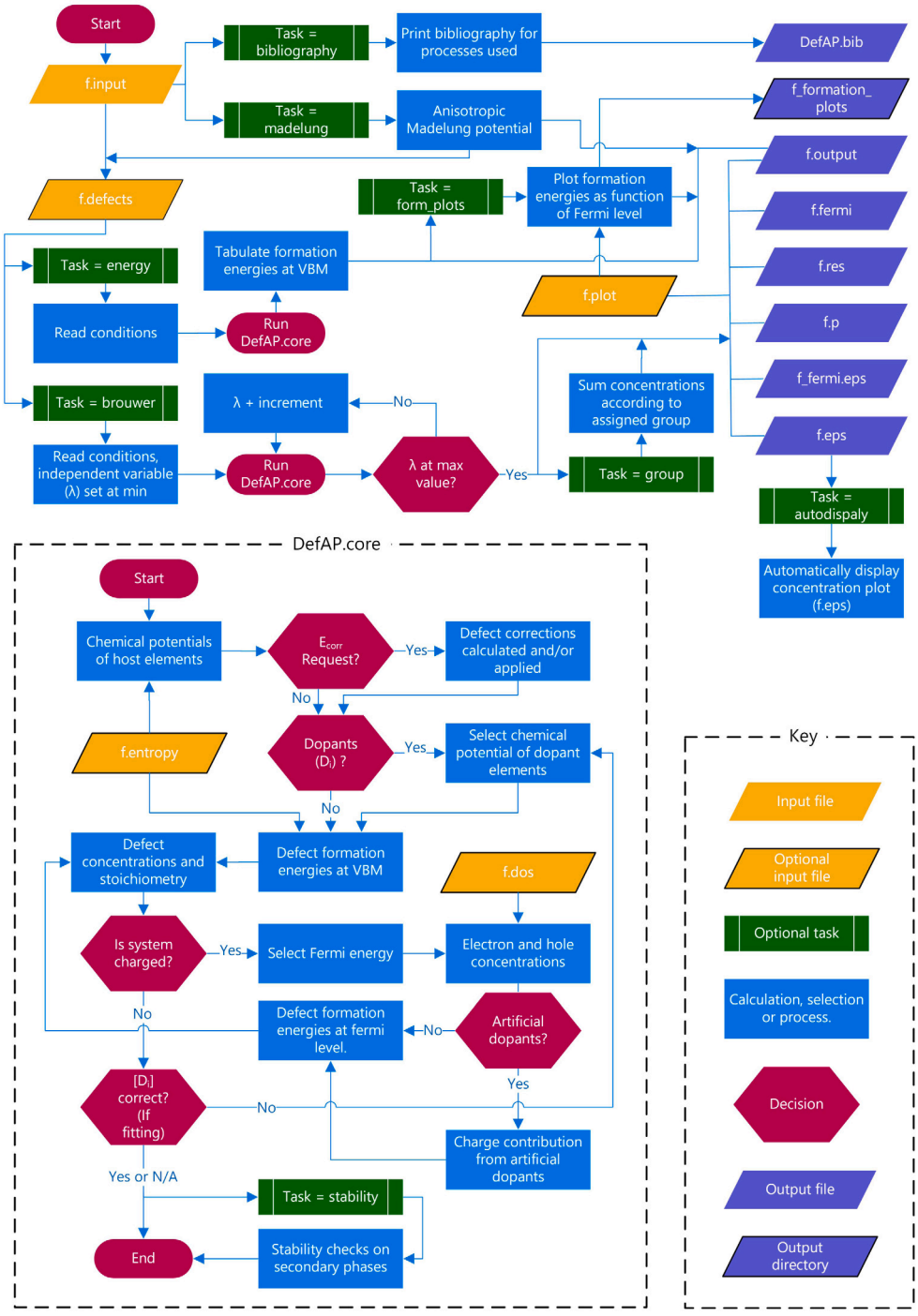

Fig. 1. DefAP flow diagram.

investigation of each is not performed. DefAP operates according to user-requested `tasks`, most of which require data acquired from first-principle calculations performed on the system of interest. This data, as well as user defined information (such as the environmental conditions of interest) is collected in the DefAP input files. Fig. 1 illustrates how DefAP operates, showing how operations performed are dependent on the `tasks` selected. DFT is employed to study the four example systems, the details of these simulations is compiled in the supplementary material. All defects in this paper are represented with Kröger–Vink notation [27], modified to display charge as an integer value (no charge indicated by: ×).

3.1. Silicon

To study intrinsic Si, we investigate the cubic diamond structure and the formation of both uncharged and charged vacancies and interstitials in several configurations. Three interstitial sites are studied: the tetrahedral ($Si_{i,T}$), hexagonal ($Si_{i,H}$), and the <110> dumbbell configuration ($Si_{i,110}$), where two Si atoms share one atom site. As well as the conventional vacancy, where one Si atom is removed from the perfect lattice ($V_{Si,L}$), a split vacancy is also considered, where a Si atom sits between two empty sites ($V_{Si,B}$). The carrier concentration is of particular importance within semiconductor materials; we use the

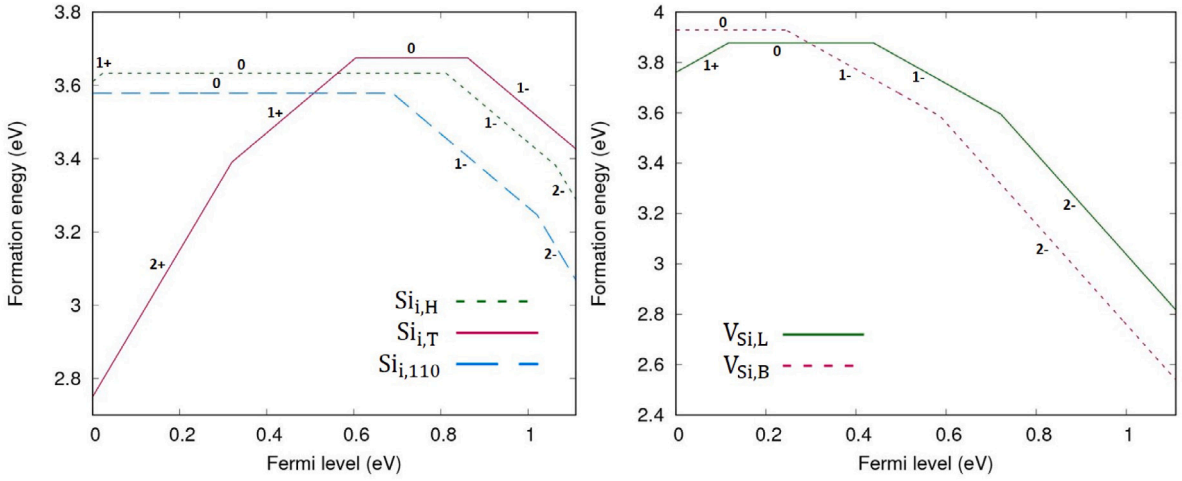

Fig. 2. Defect formation energies for intrinsic interstitials (left) and vacancies (right) in Si as a function of Fermi energy. Only the charge state with the lowest formation energy for a given Fermi level is shown for each defect, represented with numeric label.

option available in DefAP to calculate these concentrations using the DOS effective masses of the electrons and holes (Eqs. (34) and (35)). The values reported by Green [28] are used for the effective masses of electrons and holes. Green tabulated values between 50 K and 500 K, at 50 K intervals; DefAP uses an interpolation function to estimate values at temperatures falling in the intervals. A charge correction is calculated and applied to the formation energy of each charged defect, using Eq. (39) and a static dielectric constant of 11.9 [29]. The task `energy` instructs DefAP to calculate the formation energy of each defect at the VBM, and when coupled with the task `form_plots`, DefAP produces figures illustrating the defect's formation energy dependence on Fermi level across the length of the band gap, if a charged system is studied. Fig. 2 demonstrates the output of this task for the intrinsic defects studied in Si, with a separate plot for interstitials and vacancies (please note that the charge labels have been manually added). Fig. 2 shows only the charge state with the lowest formation energy for each defect, which is an optional user choice. We see that positively charged $Si_{i,T}$ interstitials have the lowest formation energy below the midpoint of the band gap, whereas neutral and negatively charged $Si_{i,110}$ interstitials are favoured above the midpoint, towards the conduction band. Negatively charged $V_{Si,B}$ vacancies are found to have lowest formation energy across the majority of the band gap. We also see that all defects have relatively high formation energies, explaining the low concentrations of intrinsic defects we see in Si. The values and trends seen in Fig. 2 are in close agreement with the DFT study of Centoni et al. [30] where the interstitial and vacancy with the lowest formation energy varied between the VBM and CBM in the order $Si^{2+}_{i,T} \rightarrow Si^{\times}_{i,110} \rightarrow Si^{1-}_{i,110}$ and $V^{1+}_{Si,L} \rightarrow V^{\times}_{Si,L} \rightarrow V^{1-}_{Si,L} \rightarrow V^{2-}_{Si,B}$, respectively.

Fig. 3 displays the output of the task `brouwer`: a plot of the defect concentrations as a function of a chosen variable, in this case, temperature. Intrinsic silicon is predicted to have a very low concentrations of defects. The carrier concentrations are equal, but none of the intrinsic defects are found to exist at a concentration above 10^{-12} cm^{-3} in the temperature range studied. Si is doped with impurity atoms to alter its properties; for example incorporation of phosphorus creates n-type Si. We replace one Si atom with a P atom to create a Si substitutional, $P^{j}_{Si,L}$, with integer j values between ± 3 considered. This substitutional was found to be the favoured accommodation site of P in Si, compared to the three interstitial sites discussed earlier. DefAP then uses the methodology described in Section 2.5 to investigate the impact of a fixed P concentration of 1×10^{15} cm^{-3} (equivalent to a concentration of approximately 2×10^{-8} P atoms per Si). Fig. 3 shows that DefAP correctly predicts that P behaves as an n-type dopant, raising the Fermi level in Si, and consequently increasing the concentration of electrons. The dominant P defect charge states are predicted to be $P^{\times}_{Si,L}$ and $P^{1+}_{Si,L}$ with the former making up the bulk of P in Si at low temperatures. The impact of adding P on the Fermi level is shown on the plot in Fig. 4. This plot, illustrating the predicted Fermi level as a function of the environmental variable selected (temperature in this case) is automatically produced by DefAP when using the task `brouwer`. We superimpose two of these plots in Fig. 4 to allow comparison.

3.2. Plutonium dioxide

The defect chemistry of the binary oxide PuO_2 is studied to improve understanding of its long-term behaviour in scenarios/applications including storage, as a component of new nuclear fuels and in radioisotope thermoelectric heaters [31–33]. Here, we study the charged intrinsic point defects of PuO_2 and use DefAP to calculate each defect's formation energy with consideration of the change in vibrational entropy each defect evokes, as outlined in Section 2.3. Vibrational entropies were obtained using empirical potentials, with the General Utility Lattice Program (GULP) [34] together with the Cooper, Rushton and Grimes (CRG) [35,36] potential; results are tabulated in the previous work [25]. The scheme of Kumagai and Oba [18] is used to calculate E_{corr}; DefAP contains an entry for each defect where the value of an externally calculated charge correction can be logged and applied in Eq. (2), should the user prefer not to use the simple point charge correction scheme available within DefAP. Fermi–Dirac statistics are used to compute the concentration of electrons and holes in the system (Eqs. (32) and (33)).

In Fig. 5, the result of the task `brouwer` for the PuO_2 system is presented. It displays the predicted defect chemistry as a function of oxygen partial pressure at a fixed temperature of 500 K, approximating storage temperatures. Fig. 5(a) shows that it is the oxygen defects that dominate the defect chemistry of PuO_2 as opposed to plutonium defects. For this system, we use the option in DefAP to calculate and plot the stoichiometry (value for x in $PuO_{2\pm x}$) on the same concentration plot, using Eq. (43). This allows us to clearly illustrate that PuO_{2+x} is unfavourable, in contrast, the degree of hypostoichiometry (PuO_{2-x}) that can be reached is significantly greater.

The properties of PuO_2 are altered by the accumulation of radiogenic impurities, with one of the most significant being americium, produced by ^{241}Pu decaying into ^{241}Am. DefAP is able to predict the impact on the defect chemistry of this ingrowth. As outlined in Section 2.5, we are able to artificially add a chosen concentration of charge to the system to mimic the presence of Am, as an alternative to performing further DFT simulations. Am (III) is predicted to be

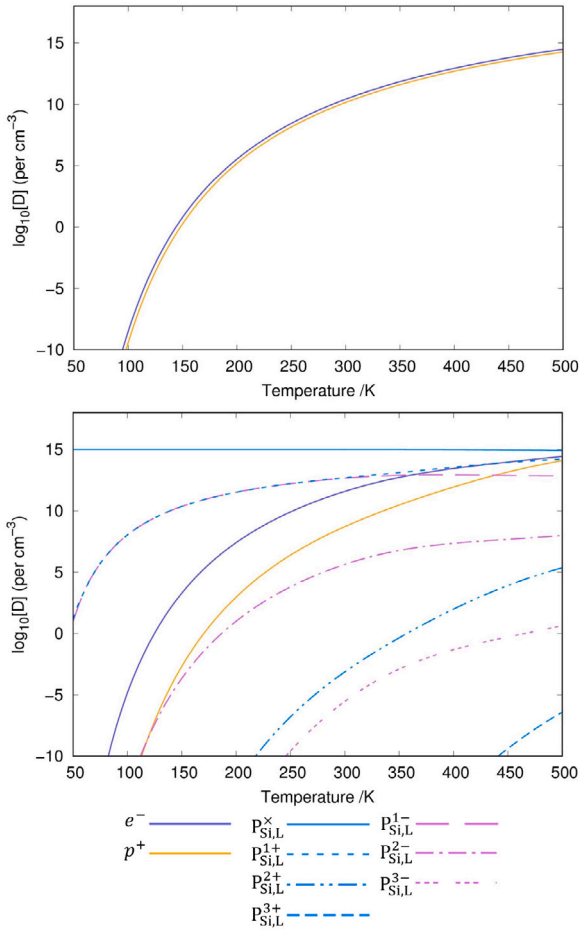

Fig. 3. The defect concentrations in Si as a function of temperature with a P concentration of (top) 0.0 and (bottom) 1×10^{15} cm^{-3} (equivalent to a concentration of approximately 2×10^{-8} P atoms per Si). The carrier concentrations are equal in the top figure, the concentration of electrons were artificially shifted in order for both lines to be visible.

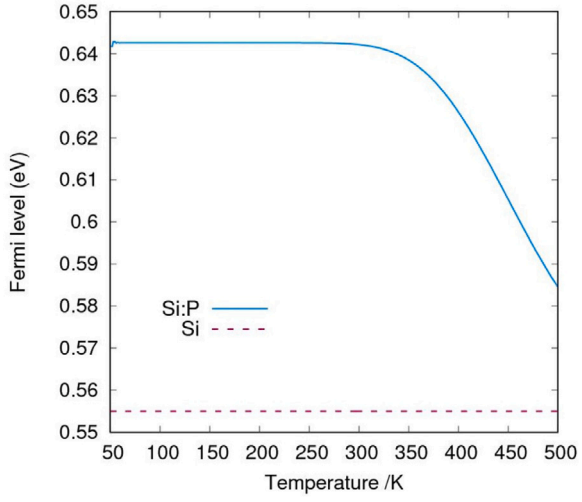

Fig. 4. The predicted Fermi level as a function of temperature in intrinsic and P-doped Si, with a P concentration of 1×10^{15} cm^{-3} (equivalent to a concentration of approximately 2×10^{-8} P atoms per Si).

accommodated in PuO_2 as substitutions on Pu sites, with a net charge of −1 (Am^{1-}_{Pu}) [37]. We therefore introduce a controlled concentration of

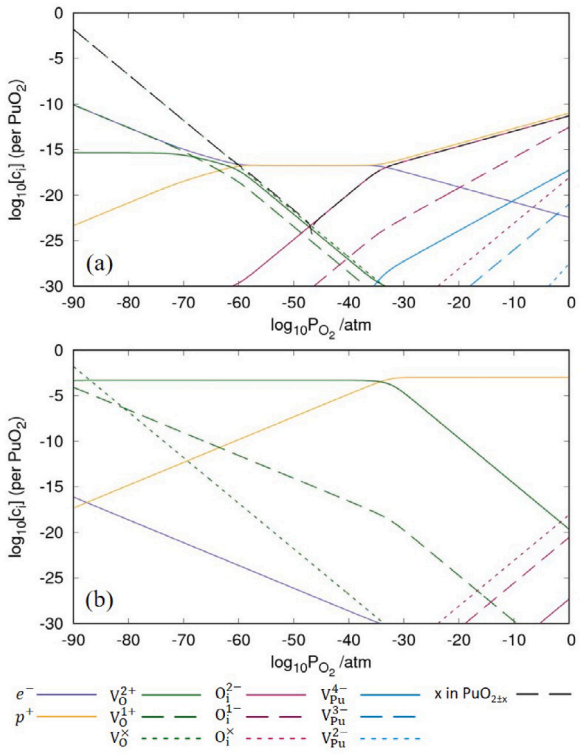

Fig. 5. The concentration of defects in PuO_2 as a function of oxygen partial pressure at 500 K. In (b), a concentration of 0.1% Am (III) in PuO_2 is simulated by adding a fixed concentration of 0.001 charges (with a charge magnitude of −1) per PuO_2.

charge, with a charge magnitude of −1, which replicates the accumulation of Am (III) in PuO_2. Fig. 5(b) demonstrates the significant impact of adding a fixed concentration of 0.001 charges (with a charge magnitude of −1) per PuO_2 has on the defect chemistry. The concentration of holes and oxygen vacancies rise by orders of magnitude in response to the presence of the Am (III) simulant.

3.3. Yttrium barium copper oxide

The critical temperature of the high temperature superconductor $YBa_2Cu_3O_7$ has been shown to be dependent upon the value of x in $YBa_2Cu_3O_{7-x}$, motivating the study of point defects in the material. Vacancies, interstitials, and antisite defects are studied, taking into account the different, unique defect sites in $YBa_2Cu_3O_7$ that are possible due to its orthorhombically shaped unit cell. Clustered oxygen vacancies are also considered: pairs of oxygen vacancies in the Cu-O chain, denoted V_{O2}, were calculated. The DFT treatment of this complex crystallography is discussed in previous work [38]. $YBa_2Cu_3O_7$ falls into the category of a non-binary volatile compound; to calculate the chemical potentials of Y, Ba, Cu, and O, DefAP uses the method outlined in Section 2.1 (Eqs. (18)–(26)), using the real heat capacities of O_2 to determine the oxygen chemical potential temperature dependence. This method requires that three binary oxides are defined (one for each metal species in the host) that $YBa_2Cu_3O_7$ could theoretically be constructed from. We select the following oxides:

$$3Cu_2O_{(s)} + 4BaO_{(s)} + Y_2O_{3(s)} + 2O_{2(g)} \rightarrow YBa_2Cu_3O_{7(s)} \quad (45)$$

Fig. 6 presents the output of the task `brouwer` for the $YBa_2Cu_3O_7$ system at 700 K, under Cu_2O-poor conditions (BaO- and Y_2O_3-rich conditions). We use the option in DefAP to plot the defect concentrations as a function of x in $YBa_2Cu_3O_{7+x}$ and for clarity, sum and plot together all defects of the same type by using the task `group` meaning that for

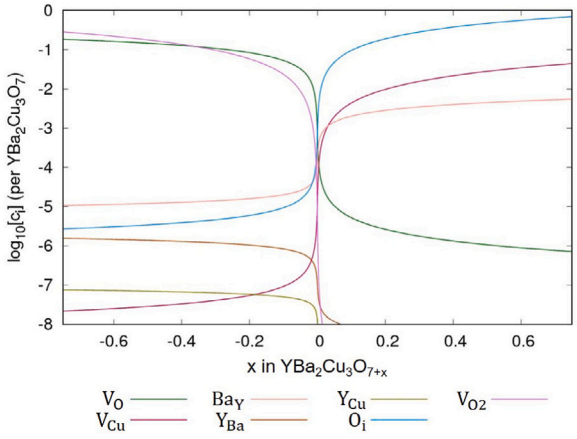

Fig. 6. The concentration of defects in $YBa_2Cu_3O_{7+x}$ as a function of x at 700 K under Cu_2O-poor conditions.

Table 1
The stability of selected competing phases in the $YBa_2Cu_3O_7$ system calculated at 700 K, an oxygen partial pressure of 10^{-4} atm, and Cu_2O-poor conditions.

Compound	$\Delta\mu$
Y_2BaO_4	0.0950
$Y_4Ba_3O_9$	−0.0798
$YCuO_2$	−0.826
YCu_2O_4	−0.425
BaCu	−6.05
$BaCu_3O_4$	−0.742
$Ba_2Cu_3O_6$	0.734
CuY	−9.69
Cu_2BaO_2	−1.16
Cu_5Y	−14.5

$\Delta\mu$ denotes the difference between the summed chemical potentials calculated by DefAP and the DFT energy of each compound. A positive $\Delta\mu$ indicates thermodynamic stability w.r.t. $YBa_2Cu_3O_7$.

example $c_{V_{Cu}} = c_{V_{Cu1}} + c_{V_{Cu2}}$. Fig. 6 enables easy interpretation of the defects that are predicted to cause oxygen deficiency in $YBa_2Cu_3O_{7-x}$: It is the oxygen vacancy defects that are responsible for the deficiency, with the clustered vacancies increasingly significant with increasing x. $YBa_2Cu_3O_7$ has a multitude of competing phases that it could possibly decompose to. Running the task `stability` evaluates the thermodynamic stability of an unlimited number of possible competing phases, requiring only the DFT energy of each compound to be defined. Checking the ten compounds in Table 1 reveals that at 700 K, an oxygen partial pressure of 10^{-4} atm, and Cu_2O-poor conditions, it is predicted that the compounds Y_2BaO_4 and $Ba_2Cu_3O_6$ are thermodynamically stable with respect to $YBa_2Cu_3O_7$: i.e. it would be thermodynamically favourable for these two phases to form as secondary phases within $YBa_2Cu_3O_7$.

3.4. Lithium metatitanate

Li_2TiO_3, is a leading candidate tritium breeding material for use in a future fusion reactor. The material generates tritium by transmutation of the Li induced by the neutron produced in the fusion reaction: ${}^{7}_{3}\mathrm{Li} + {}^{1}_{0}n \rightarrow {}^{4}_{2}\mathrm{He} + {}^{3}_{1}\mathrm{T} + {}^{1}_{0}n$. With use of the SLSQP algorithm implemented in DefAP, we study the accommodation method of defined quantities of both He and T concurrently, as well as their impact on the intrinsic defect chemistry of Li_2TiO_3. To attain the chemical potentials of the host elements, Li, Ti and O, DefAP repeats the method described for $YBa_2Cu_3O_7$ (also a non-binary compound) using the following oxides to thermodynamically construct Li_2TiO_3:

$$Li_2O_{(s)} + TiO_{2(s)} \rightarrow Li_2TiO_{3(s)} \tag{46}$$

Continuing from previous work [39,40], we investigate each conceivable intrinsic defect at every unique site in the Li_2TiO_3 unit cell and at all accessible charge states. Li and O substitutions, as well as interstitial sites, are considered here as the possible T and He incorporation sites. To calculate the concentration of electrons and holes, Boltzmann statistics are selected (Eqs. (30) & (31)). Li_2TiO_3 is an example of a non-cubic system that exhibits anisotropic dielectric properties, necessitating careful consideration of the charge correction assigned to the charged defects studied. The task `madelung` is used to calculate v_M^{scr} for Li_2TiO_3, using Eq. (40) and the dielectric tensor predicted by Murphy and Hine [17], thereby accounting for the anisotropic nature of Li_2TiO_3:

$$\bar{\epsilon} = \begin{bmatrix} 36.1 & 0 & -5.0 \\ 0 & 37.8 & 0 \\ -5.0 & 0 & 17.8 \end{bmatrix} \tag{47}$$

DefAP automatically uses the v_M^{scr} calculated to apply a charge correction (Eq. (39)) when computing the formation energies of the charged defects in subsequent tasks. The result of the task `brouwer`, with the task `group` used to sum defects of the same type that vary only in position in the cell, is shown in Fig. 7. The plots shows the concentration of defects in Li_2TiO_3 at 1000 K under either Li_2O- or TiO_2-rich conditions. Figs. 7a & b show that when both T and He concentrations are fixed at 0.01 atoms per Li_2TiO_3 functional unit, T is incorporated as either T_O^{1+} or T_i^{1+} defects in Li_2O-rich conditions, and $T_{Li}^{\times}$ defects in TiO_2-rich conditions. Meanwhile, He is incorporated as either He_O^{2+} or $He_i^{\times}$ defects in Li_2O-rich conditions, and He_{Li}^{1-} defects in TiO_2-rich conditions. So far, this result is indicative that the presence of T or He in Li_2TiO_3 does not affect the method of incorporation of the other impurity; the methods of incorporation are not predicted to be altered compared to when T and He have been studied individually [39,40]. This can be further explored by using the option in DefAP to study defect concentrations as a function of a chosen dopant element concentration. In Figs. 7c & d, the defect concentrations in Li_2TiO_3 are plotted as a function of T concentration, with He concentration fixed at 0.01 atoms per Li_2TiO_3 functional unit. We now see that, in Li_2O-rich conditions, the quantity of T present does impact the mode of He accommodation. At low T concentrations, He is accommodated as both $He_i^{\times}$ and He_O^{2+} defects. However, increasing the total concentration of T present results in only the $He_i^{\times}$ being favourable. This is due to the T being accommodated as the positively charged T_i^{1+} defect, therefore, as this increases to ensure charge neutrality the concentration of He_O^{2+} must decrease. In contrast, the equivalent result at TiO_2-rich conditions finds that the concentration of T has no bearing on the mode of He incorporation, due to the dominant $T_{Li}^{\times}$ defect being charge neutral. The intrinsic defect chemistry of Li_2TiO_3 is also predicted to respond in response to increasing He concentrations: charge compensation for the T_i^{1+} defect is provided by increasing the concentration of the Li_{Ti}^{3-} defect.

4. Conclusion

We have introduced DefAP, a Python code designed to analyse a material's defect chemistry by processing the results of DFT calculations according to the instructions of the user, generating an output of plots designed with gnuplot. This paper has used example systems to demonstrate the flexibility and capabilities of the code. The formation energies of charged intrinsic defects in Si as a function of Fermi level were predicted, whilst the equilibrium concentration of defects, and carriers where applicable, were studied in Si, PuO_2, $YBa_2Cu_3O_7$, and Li_2TiO_3. A suitable point charge correction can be calculated on request in the event charged defects are studied, that is applicable to both isotropic and anisotropic systems. DefAP has an extensive set of options

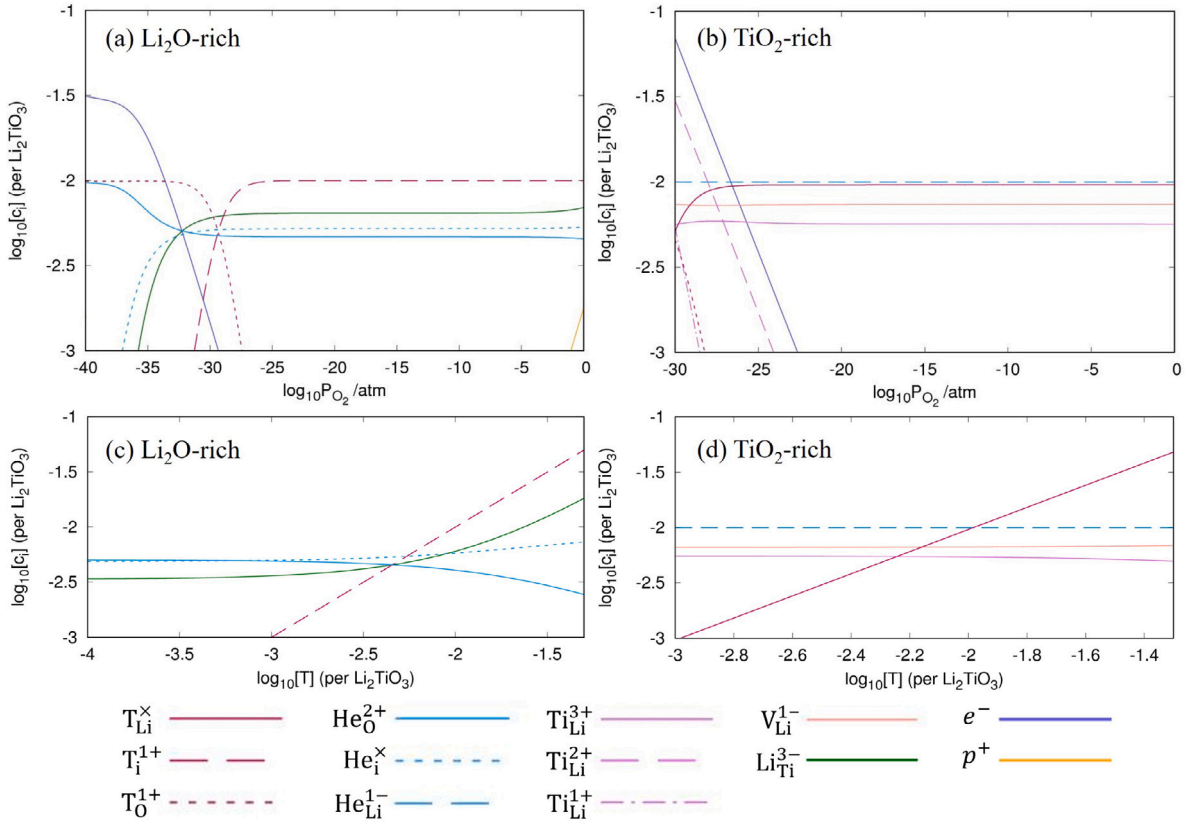

Fig. 7. The concentration of defects in Li_2TiO_3 at 1000 K under Li_2O and TiO_2-rich conditions. In (a) and (b) concentrations are plotted as a function of oxygen partial pressure with the total concentration of T and He fixed at 0.01 atoms per Li_2TiO_3 functional unit. In (c) and (d) concentrations are plotted as a function of the total concentration of T, with the total concentration of He fixed at 0.01 atoms per Li_2TiO_3 functional unit and an oxygen partial pressure of 10^{-20} atm.

for studying dopants, here we studied the dopant P in Si, the decay-product Am in PuO_2, and the breeder products T and He in Li_2TiO_3. The package is available on GitHub at https://github.com/DefAP/defap.

CRediT authorship contribution statement

William D. Neilson: Software, Formal analysis, Validation, Writing – original draft. **Samuel T. Murphy:** Conceptualisation, Software, Writing – review & editing, Supervision, Funding acquisition.

Declaration of competing interest

The authors declare that they have no known competing financial interests or personal relationships that could have appeared to influence the work reported in this paper.

Data availability

The raw/processed data required to reproduce these findings are available to download from https://github.com/DefAP/defap.

Acknowledgements

This work was completed using the High End Computing facility at Lancaster University. This project was funded as part of EPSRCs TRANSCEND, UK project (EP/S01019X/1).

Appendix A. Supplementary data

Supplementary material related to this article can be found online at https://doi.org/10.1016/j.commatsci.2022.111434.

The DFT simulation parameters for the work conducted in this paper are compiled in the supplementary document.

References

[1] M. Stoneham (Ed.), Theory of Defects in Solids: Electronic Structure of Defects in Insulators and Semiconductors, Oxford University Press, Oxford, UK.
[2] J. Spitaler, S.K. Estreicher, Perspectives on the theory of defects, Front. Mater. 5 (2018) 70, http://dx.doi.org/10.3389/fmats.2018.00070.
[3] C.G. de Walle, A. Janotti, Advances in electronic structure methods for defects and impurities in solids, Phys. Status Solidi B 248 (1) (2011) 19–27, http://dx.doi.org/10.1002/pssb.201046290.
[4] S. Kim, S.N. Hood, J.-S. Park, L.D. Whalley, A. Walsh, Quick-start guide for first-principles modelling of point defects in crystalline materials, J. Phys. Energy 2 (3) (2020) 36001, http://dx.doi.org/10.1088/2515-7655/aba081.
[5] J.L. Lyons, C.G. de Walle, Computationally predicted energies and properties of defects in GaN, NPJ Comput. Mater. 3 (2017) 12.
[6] A. Goyal, P. Gorai, H. Peng, S. Lany, V. Stevanović, A computational framework for automation of point defect calculations, Comput. Mater. Sci. 130 (2017) 1–9, http://dx.doi.org/10.1016/j.commatsci.2016.12.040.
[7] D. Broberg, B. Medasani, N.E.R. Zimmermann, G. Yu, A. Canning, M. Haranczyk, M. Asta, G. Hautier, PyCDT: A Python toolkit for modeling point defects in semiconductors and insulators, Comput. Phys. Comm. 226 (2018) 165–179, http://dx.doi.org/10.1016/j.cpc.2018.01.004.
[8] M. Arrigoni, G.K.H. Madsen, Spinney: Post-processing of first-principles calculations of point defects in semiconductors with Python, Comput. Phys. Comm. 264 (2021) 107946, http://dx.doi.org/10.1016/j.cpc.2021.107946.
[9] A. Stoliaroff, S. Jobic, C. Latouche, PyDEF 2.0: An easy to use post-treatment software for publishable charts featuring a graphical user interface, J. Comput. Chem. 39 (26) (2018) 2251–2261, http://dx.doi.org/10.1002/jcc.25543.
[10] J. Buckeridge, Equilibrium point defect and charge carrier concentrations in a material determined through calculation of the self-consistent Fermi energy, Comput. Phys. Comm. 244 (2019) 329–342, http://dx.doi.org/10.1016/j.cpc.2019.06.017.
[11] W.B. Fowler, Point defects, in: F. Bassani, G.L. Liedl, P. Wyder (Eds.), Encyclopedia of Condensed Matter Physics, Elsevier, Oxford, 2005, pp. 318–323, http://dx.doi.org/10.1016/B0-12-369401-9/00412-5.
[12] M. Leslie, N.J. Gillan, The energy and elastic dipole tensor of defects in ionic crystals calculated by the supercell method, J. Phys. C: Solid State Phys. 18 (1985) 973–982, http://dx.doi.org/10.1088/0022-3719/18/5/005.

[13] G. Makov, M.C. Payne, Periodic boundary conditions in ab initio calculations, Phys. Rev. B 51 (7) (1995) 4014–4022, http://dx.doi.org/10.1103/PhysRevB.51.4014.
[14] S. Lany, A. Zunger, Assessment of correction methods for the band-gap problem and for finite-size effects in supercell defect calculations: Case studies for ZnO and GaAs, Phys. Rev. B 78 (23) (2008) 235104, http://dx.doi.org/10.1103/PhysRevB.78.235104.
[15] C. Freysoldt, J. Neugebauer, C.G. Van de Walle, Fully *ab initio* finite-size corrections for charged-defect supercell calculations, Phys. Rev. Lett. 102 (2009) 016402, http://dx.doi.org/10.1103/PhysRevLett.102.016402.
[16] S.E. Taylor, F. Bruneval, Understanding and correcting the spurious interactions in charged supercells, Phys. Rev. B 84 (7) (2011) 75155, http://dx.doi.org/10.1103/PhysRevB.84.075155.
[17] S.T. Murphy, N.D.M. Hine, Anisotropic charge screening and supercell size convergence of defect formation energies, Phys. Rev. B 87 (9) (2013) 94111, http://dx.doi.org/10.1103/PhysRevB.87.094111.
[18] Y. Kumagai, F. Oba, Electrostatics-based finite-size corrections for first-principles point defect calculations, Phys. Rev. B 89 (2014) 195205, http://dx.doi.org/10.1103/PhysRevB.89.195205.
[19] S. Kasamatsu, T. Tada, S. Watanabe, Theoretical analysis of space charge layer formation at metal/ionic conductor interfaces, Solid State Ion. 183 (1) (2011) 20–25, http://dx.doi.org/10.1016/j.ssi.2010.11.022.
[20] M.W. Finnis, A.Y. Lozovoi, A. Alavi, The oxidation of NiAl: What can we learn from Ab initio calculations? Annu. Rev. Mater. Res. 35 (2005) 167–207, http://dx.doi.org/10.1146/annurev.matsci.35.101503.091652.
[21] P. Linstrom, W. Mallard (Eds.), NIST Chemistry WebBook, NIST Standard Reference Database Number 69, National Institute of Standards and Technology, Gaithersburg, MD 20899.
[22] M.W.D. Cooper, S.T. Murphy, D.A. Andersson, The defect chemistry of $UO_{2\pm x}$ from atomistic simulations, J. Nucl. Mater. 504 (2018) 251–260, http://dx.doi.org/10.1016/j.jnucmat.2018.02.034.
[23] A. Soulié, F. Bruneval, M.-C. Marinica, S. Murphy, J.-P. Crocombette, Influence of vibrational entropy on the concentrations of oxygen interstitial clusters and uranium vacancies in nonstoichiometric UO_2, Phys. Rev. Mater. 2 (2018) 083607, http://dx.doi.org/10.1103/PhysRevMaterials.2.083607.
[24] R. Perriot, C. Matthews, M.W.D. Cooper, B.P. Uberuaga, C.R. Stanek, D.A. Andersson, Atomistic modeling of out-of-pile xenon diffusion by vacancy clusters in UO_2, J. Nucl. Mater. 520 (2019) 96–109, http://dx.doi.org/10.1016/j.jnucmat.2019.03.050.
[25] W.D. Neilson, J.T. Pegg, H. Steele, S.T. Murphy, The defect chemistry of non-stoichiometric $PuO_{2\pm x}$, Phys. Chem. Chem. Phys. 23 (8) (2021) 4544–4554, http://dx.doi.org/10.1039/D0CP06497A.
[26] T.R. Durrant, S.T. Murphy, M.B. Watkins, A.L. Shluger, Relation between image charge and potential alignment corrections for charged defects in periodic boundary conditions, J. Chem. Phys. 149 (2018) 024103, http://dx.doi.org/10.1063/1.5029818.
[27] F.A. Kröger, H.J. Vink, Relations between the concentrations of imperfections in crystalline solids, in: F. Seitz, D. Turnbull (Eds.), in: Solid State Physics, vol. 3, Academic Press, 1956, pp. 307–435, http://dx.doi.org/10.1016/S0081-1947(08)60135-6.
[28] M.A. Green, Intrinsic concentration, effective densities of states, and effective mass in silicon, J. Appl. Phys. 67 (6) (1990) 2944–2954, http://dx.doi.org/10.1063/1.345414.
[29] S.M. Sze, in: K.K. Ng (Ed.), Physics of Semiconductor Devices, third ed., Wiley-Interscience, 2007.
[30] S.A. Centoni, B. Sadigh, G.H. Gilmer, T.J. Lenosky, T. de la Rubia, C.B. Musgrave, First-principles calculation of intrinsic defect formation volumes in silicon, Phys. Rev. B 72 (19) (2005) 195206, http://dx.doi.org/10.1103/PhysRevB.72.195206.
[31] G. Bailey, E. Bluhm, J. Lyman, R. Mason, M. Paffett, G. Polansky, G.D. Roberson, M. Sherman, K. Veirs, L. Worl, Gas Generation from Actinide Oxide Materials, Tech. Rep. LA-13781-MS, Los Alamos National Laboratory, Los Alamos, NM, 2000, p. 72.
[32] Nuclear Decommissioning Authority, 2019, Progress on Plutonium Consolidation, Storage and Disposition, Tech. Rep, 2019.
[33] R.C. O'Brien, R.M. Ambrosi, N.P. Bannister, S.D. Howe, H.V. Atkinson, Safe radioisotope thermoelectric generators and heat sources for space applications, J. Nucl. Mater. 377 (2008) 506–521, http://dx.doi.org/10.1016/j.jnucmat.2008.04.009.
[34] J.D. Gale, GULP: A Computer program for the symmetry-adapted simulation of solids, J. Chem. Soc. Faraday Trans. 93 (1997) 629–637, http://dx.doi.org/10.1039/A606455H.
[35] M.W.D. Cooper, M.J.D. Rushton, R.W. Grimes, A many-body potential approach to modelling the thermomechanical properties of actinide oxides, J. Phys.: Condens. Matter 26 (2014) 105401, http://dx.doi.org/10.1088/0953-8984/26/10/105401.
[36] M.W.D. Cooper, S.T. Murphy, M.J.D. Rushton, R.W. Grimes, Thermophysical properties and oxygen transport in the $(U_x,Pu_{1-x})O_2$ lattice, J. Nucl. Mater. 461 (2015) 206–214, http://dx.doi.org/10.1016/j.jnucmat.2015.03.024.
[37] W.D. Neilson, H. Steele, S.T. Murphy, Evolving defect chemistry of $(Pu,Am)O_{2\pm x}$, J. Phys. Chem C 125 (28) (2021) 15560–15568, http://dx.doi.org/10.1021/acs.jpcc.1c03274.
[38] S.T. Murphy, A point defect model for $YBa_2Cu_3O_7$ from density functional theory, J. Phys. Commun. 4 (11) (2020) 115003, http://dx.doi.org/10.1088/2399-6528/abc9a7.
[39] S.T. Murphy, N.D.M. Hine, Point defects and non-stoichiometry in Li_2TiO_3, Chem. Mater. 26 (2014) 1629–1638, http://dx.doi.org/10.1021/cm4038473.
[40] S.T. Murphy, Mechanisms of helium accommodation in lithium metatitanate, Fusion Eng. Des. 101 (2015) 94–100, http://dx.doi.org/10.1016/j.fusengdes.2015.10.007.